

Automatic TFT-LCD mura defect inspection using discrete cosine transform-based background filtering and 'just noticeable difference' quantification strategies

Liang-Chia Chen and Chia-Cheng Kuo

Graduate Institute of Automation Technology, National Taipei University of Technology,
No 1, Sec. 3, Chung Hsiao E. Rd, Taipei 106, Taiwan

E-mail: lcchen@ntut.edu.tw

Received 13 April 2007, in final form 6 October 2007

Published 30 November 2007

Online at stacks.iop.org/MST/19/015507

Abstract

An innovative mura defect detection methodology for a thin-film transistor liquid crystal display (TFT-LCD) is developed for automatic inspection of mura defects using the discrete cosine transform (DCT) principle and background image filtering strategy. Efficient and accurate surface defect detection on flat panel display (FPD) panels has never been so important in achieving a high yield rate of FPD manufacturing. Detecting blob-mura defects in an LCD panel can be difficult due to non-uniform brightness background and slightly different brightness levels between the defect region and the background. To overcome this problem, a DCT-based background reconstruction algorithm was developed to establish the background image separated from the defects. The significant level of mura defects can be rationally quantified using the just noticeable difference (JND) definition. Actual performance of the developed method was evaluated on industrial LCD panels containing natural mura defects. Results of experimental tests verified that the proposed algorithm has a superior capability for detecting mura defects efficiently and accurately.

Keywords: automatic optical inspection (AOI), defect inspection, TFT-LCD, discrete cosine transform (DCT), mura defects.

(Some figures in this article are in colour only in the electronic version)

1. Introduction

Manufacturers of all kinds of flat panel displays (FPDs) need to inspect products such as screen panels, control PCBs and final assembly modules. Front-of-screen (FOS) quality performed by manual visual inspection may result in unacceptable manufacturing costs and uncertain product delivery time. Therefore, automatic inspection of FOS quality is highly essential to achieve effective defect detection for optimizing operation efficiency and product quality. One of the most difficult problems in visual inspection of LCD panels

involves the distinction of specific regions of low-contrast and non-uniform brightness, known as 'mura'. Mura defects are generally caused by undesired optical non-uniformity from many possible sources, such as backlight modules, TFT array layers, colour filters, coplanarity (or uniformity of the device height) of photon spacers between glasses, liquid crystal or polarizers [1]. A mura defect possesses a region of non-uniform brightness that differs slightly from the background by down-to-unit signal level, where it is detectable only when its size is larger than a specific size [2]. Therefore, detecting blob-mura defects in an LCD panel can be difficult due to the

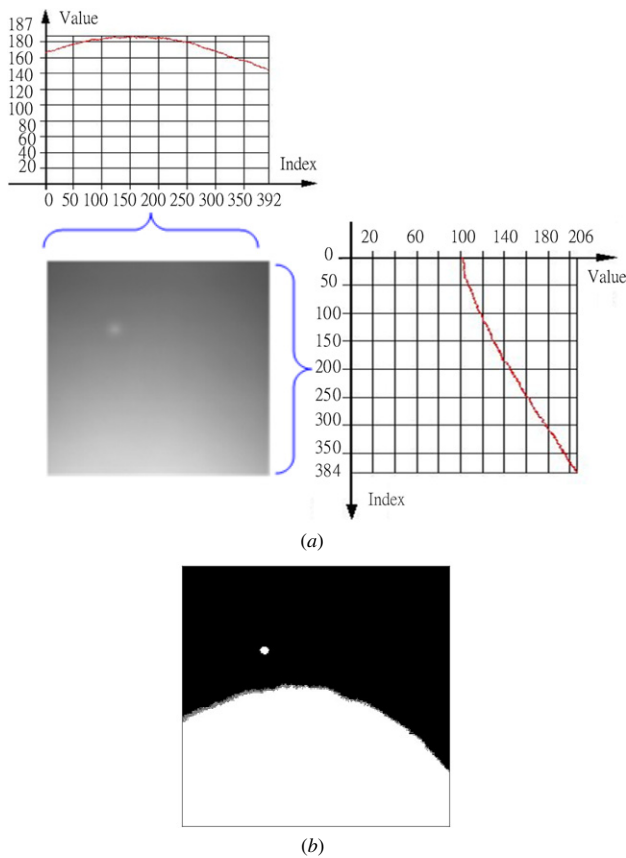


Figure 1. Illustration of TFT-LCD panel images: (a) distribution of gray values of a TFT-LCD panel along horizontal and vertical directions and (b) problematic results of display quality inspection using direct image segmentation.

inherent non-uniformity of the background brightness being comparable to the tiny slight difference in brightness levels between the defect region and the background. The example seen in figure 1(a) is an LCD screen having non-uniform lighting condition that cannot be effectively inspected using a conventional image segmentation approach. The image background is easily mixed with mura defects, as shown in figure 1(b). It is of urgent need to develop automatic mura detection with the capability of clear separation from the background image.

2. Literature review

Defect inspection strategies have recently been developed to overcome challenges in detecting mura defects from LCD images with non-uniform brightness. Song first developed a circle kernel for detecting blob effects of various sizes and a morphology-based preprocessing method for improving the detection capacity [3]. However, the method is limited to circle-type defects and cannot be applied to mura of general type. To resolve this, Lee suggested a regression fitting strategy for reconstructing the background without influence from mixing with mura defects [4]. Then again, owing to excessive operation time consumed in regression fitting, Lee’s

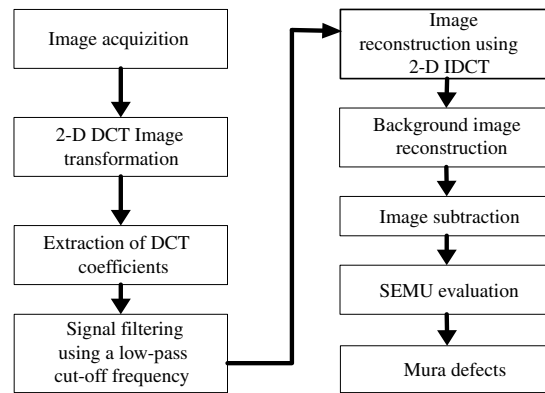


Figure 2. DCT algorithm developed for mura detection.

method is impractical for real work in the field. Different from previous methods, Kim’s approach applied white light and Fourier filter lens to filter regular fringe patterns for achieving superior detection efficiency [5]. Unfortunately, it cannot be employed to detect mura defects due to hardware limitations. To resolve this, a discrete cosine transform (DCT)-based background reconstruction algorithm was developed to establish the background image separated from mura regions to be detected. The objective of this research was to establish an efficient and effective detection and quantification methodology for LCD mura defects.

3. Methodology for mura detection

Figure 2 illustrates the flow chart of the developed methodology, a segmentation approach to the detection of area muras. The background of the inspected images is first extracted and reconstructed using the DCT principle and an image filtering strategy. Mura defects can then be detected and quantified by the developed segmentation strategy. An LCD image acquired from TFT LCD cell processes is first transformed to its frequency domain and then filtered by a low-pass filtering strategy developed to extract its principal image component. Inverse discrete cosine transform (IDCT) is then utilized to reconstruct the background image. To extract mura defects, image subtraction is employed to separate defects from the background image. Following this, mura defect level is then quantified by the just noticeable difference (JND) definition developed by SEMI (Semiconductor Equipment and Materials International). Each step used in the methodology is detailed in the following subsections.

3.1. Development of hardware system for mura inspection

Figure 3 is the schematic diagram of the developed hardware system for automatic mura inspection. The LCD panel is illuminated by a controlled backlight and inspected under the condition of a dark room. The system comprises a backlight controlling module, an X–Y–Z scanning unit, a CCD camera and a personal computer. The TFT LCD module is automatically installed by an automated loading and unloading unit into the hub of the backlight controlling module for

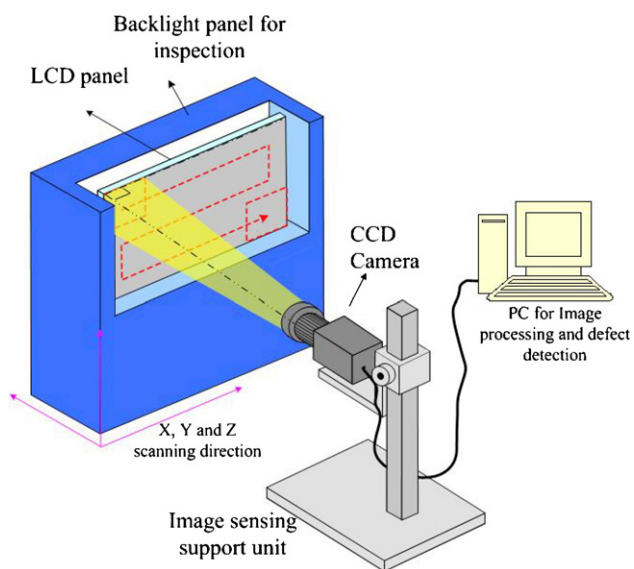


Figure 3. Schematic diagram of the hardware system developed for automatic mura inspection.

accurate positioning. Because the size of the TFT LCD panel is too big to be inspected by one single field-of-view for image sensing, the scanning unit is employed to position the panel continuously against the CCD for sequential image acquisition (shown as the dashed line with the arrow indicating the path of movement). A progressive scan Basler CCD (model A201b) with a pixel resolution of 1008×1018 and a 12-bit dynamic range resolution is employed to acquire panel images. The CCD camera is orientated by the scanning unit to be perpendicular to the LCD surface plane and the CCD image plane is focused on the surface of the LCD for best image acquisition. It is important that the luminance accuracy of the inspection system should be kept within $\pm 0.01 \text{ cd m}^{-2}$ at 100 cd m^{-2} , in order to maintain measurement repeatability. A lighting luminance control module equipped with a PWM closed-loop feedback control scheme and high-accuracy light intensity sensing capability is applied to achieve

the requirements. This luminance control applies to the acquisition of a set of sub-images to make up a whole panel image. Meanwhile, the acquired image is controlled to be similar to human perception with an infrared filter placed in front of the CCD for elimination of undesired light elements.

In the approach, the CCD acquired image is not divided into sub-image blocks due to the following three important considerations.

- (1) To avoid the area mura defects being undesirably segmented into small mura regions with less defect severity.
- (2) To establish the background image which represents the actual (or original) gray-value distribution of the tested LCD panel image.
- (3) To avoid generating any block artifact caused by merging several non-overlapping image blocks.

However, because the size of the LCD panel is usually increased for manufacturing purposes, the FOV size of the acquired image is often smaller than the panel to be inspected. Thus, the tested image has to be separated into several sub-images by the inspection system, in which sub-images must be properly merged with each other by aligning overlapped image boundaries. Accurate positioning of the LCD panel against the CCD is essential to ensure the accuracy of image merging. Meanwhile, image matching is also useful to improve the quality of the merging operation.

Another important image processing operation required for a TFT LCD panel inspection is to remove the undesired image noise caused by the black matrix (BM). The functionality of the BM of a color filter is to increase the contrast ratio of an LCD panel and to shield light leakage due to the reverse domain of liquid crystal molecules [6]. The BM is employed to isolate three colors: red, green and blue. Owing to the high detection resolution of the image acquisition, the subpixeling image of the BM can be undesirably detected and mixed with the tested image, as shown in figure 4(a), which is an example of real inspected images. To eliminate the undesired BM image, a low-pass convolution 3×3 mask is

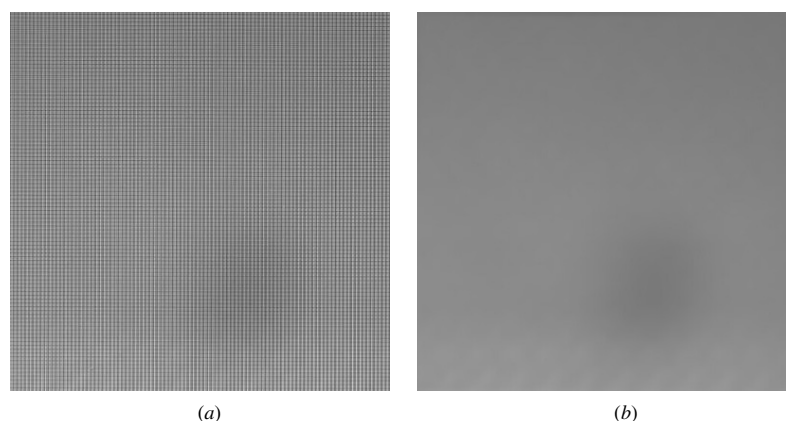


Figure 4. Example of an acquired LCD panel image: (a) the raw image without filtering undesired image element caused by black matrices and (b) the filtered image.

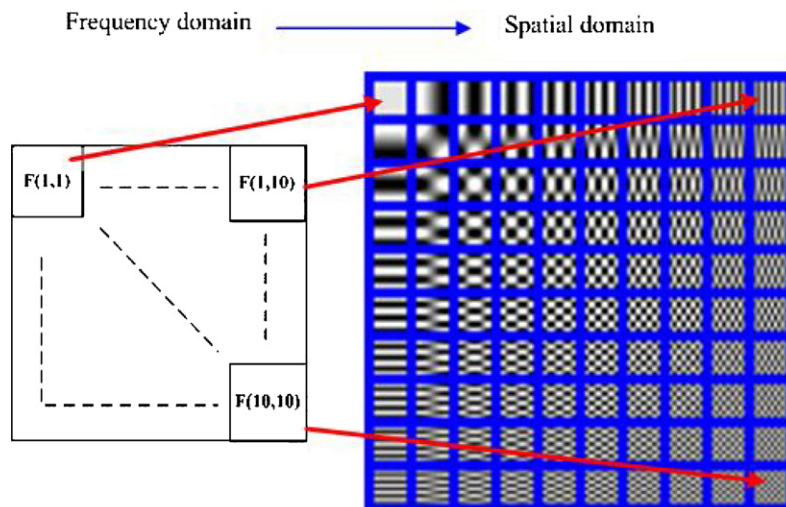


Figure 5. Basic frequency image components generated by 2D DCT.

proposed to filter the raw image as follows:

$$I'(i, j) = \frac{1}{9} \sum_{(i,j) \in w} I(i, j) \quad (1)$$

where w is the size of the convolution operation.

The result of applying the above image filtering mask to the example (figure 4(a)) is shown in figure 4(b), in which the noise caused by the BM has been effectively removed and a mura defect has been securely retained in the tested image for further defect inspection. The low-pass filter proposed is an averaged convolution operator which tends to filter out the high-frequency image component. Thus, micro defects with tiny brightness variation from the background could be easily eliminated by performing such filtering. Fortunately, mura defects normally represent a non-uniform brightness region with an image size much larger than that of micro defects. Although the boundary of the mura could be slightly reduced, most of the defects to be detected can be retained in the inspected image. Another useful method using multiple image acquisition can be applied to overcome the above issue. It sequentially acquires the LCD panel image three times, where each time the red, green and blue color elements of each pixel are lit up by a light function generator. Three acquired images are then merged to generate a BM-free panel image. This method is capable of even detecting micro defects; however, the method could consume more time for image acquisition and merging during the overall inspection cycle.

3.2. Principle of discrete cosine transform (DCT)

The DCT definition of a 1D sequence of length N of a discrete function $f(x)$, such as image gray values, can be commonly defined as [7]

$$C(u) = \alpha(u) \sum_{x=0}^{N-1} f(x) \cos \left[\frac{\pi(2x+1)u}{2N} \right] \quad (2)$$

where $x = 0, 1, 2, \dots, N - 1$;

$$\alpha(u) = \begin{cases} \sqrt{\frac{1}{N}} & \text{for } u = 0 \\ \sqrt{\frac{2}{N}} & \text{for } u \neq 0. \end{cases}$$

Similarly, the inverse transformation of $C(u)$ is defined as

$$f(x) = \alpha(u) \sum_{u=0}^{N-1} C(u) \cos \left[\frac{\pi(2x+1)u}{2N} \right] \quad (3)$$

where $x = 0, 1, 2, \dots, N - 1$;

$$\alpha(u) = \begin{cases} \sqrt{\frac{1}{N}} & \text{for } u = 0 \\ \sqrt{\frac{2}{N}} & \text{for } u \neq 0. \end{cases}$$

The first waveform ($u = 0$) stands for a constant (DC) value, whereas all other waveforms ($u = 1, 2, \dots, N - 1$) are of progressively increasing frequencies [8]. These orthogonal waveforms are called the cosine basis function, as shown in figure 5. It is important to note that the basis functions can be pre-computed offline and then multiplied with the sub-sequences, thus reducing the number of mathematical operations and significantly enhancing computation efficiency in transformation [9]. The 2D basis functions can also be generated by multiplying the horizontally oriented 1D basis functions with a vertically oriented set of the same functions.

Because the LCD image to be inspected could be of an uneven boundary, the type of DCT applied in our approach must be capable of manipulating an image with an uneven boundary. Thus, shown in equation (4), the type II DCT is applied in the approach, where the image size to be processed can be of an arbitrary $M \times N$ image region. Correspondingly, the 2D DCT is a direct extension of the 1D case and can be

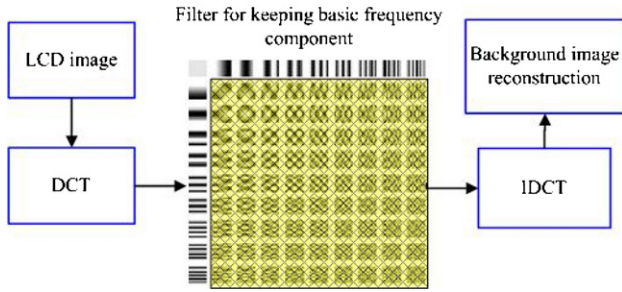


Figure 6. Design of filters by considering only the horizontal and vertical energy components.

expressed as [7]

$$C(u, v) = \alpha(u)\alpha(v) \sum_{x=0}^{M-1} \sum_{y=0}^{N-1} f(x, y) \times \cos \left[\frac{\pi(2x+1)u}{2M} \right] \cos \left[\frac{\pi(2y+1)v}{2N} \right] \quad (4)$$

where

$$\begin{aligned} x &= 0, 1, 2, \dots, M-1; & y &= 0, 1, 2, \dots, N-1; \\ u &= 0, 1, 2, \dots, M-1; & v &= 0, 1, 2, \dots, N-1; \end{aligned}$$

$$\alpha(u) = \begin{cases} \sqrt{\frac{1}{M}} & \text{for } u = 0 \\ \sqrt{\frac{2}{M}} & \text{for } u \neq 0. \end{cases}$$

$$\alpha(v) = \begin{cases} \sqrt{\frac{1}{M}} & \text{for } v = 0 \\ \sqrt{\frac{2}{M}} & \text{for } v \neq 0. \end{cases}$$

In accordance with the one-dimensional inverse transformation, the 2D inverse transform is defined as

$$f(x, y) = \sum_{u=0}^{M-1} \sum_{v=0}^{N-1} \alpha(u)\alpha(v)C(u, v) \times \cos \left[\frac{\pi(2x+1)u}{2M} \right] \cos \left[\frac{\pi(2y+1)v}{2N} \right]. \quad (5)$$

3.3. Filter design for background image reconstruction

Since the frequency characteristics of mura defects are obviously different from those of the background image, the background image can be effectively separated from the images using the DCT. In the DCT, the image components, $C(0, v)$ and $C(u, 0)$, correspond to the basic frequency image component, representing the principal image elements. Shown in figure 6, the LCD image can be decomposed into some sub-images by deploying the DCT with a filtering process. By keeping the principal frequency along the u and v directions and neglecting the other frequency components, the background of the original image separated from mura defects can be approximately reconstructed. The proposed filter is expressed as follows:

$$C_{hv}(u, v) = \begin{cases} C(u, v), & u = 0 \text{ or } v = 0 \\ 0, & \text{otherwise} \end{cases} \quad (6)$$

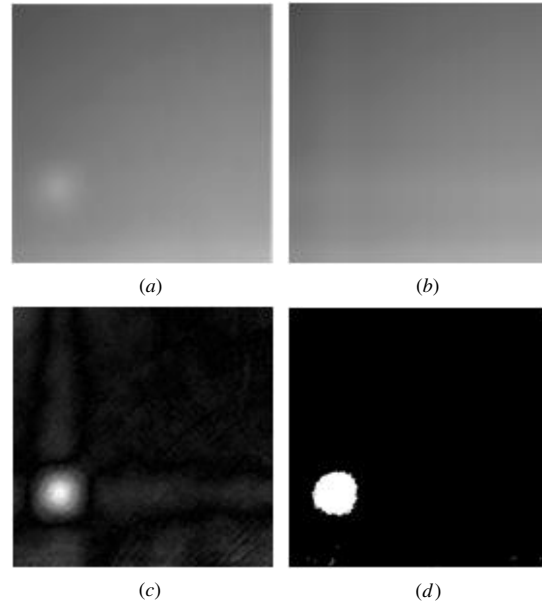


Figure 7. Detection results using the image filter proposed in figure 6: (a) the original image; (b) the reconstructed background image; (c) the net image; and (d) the detected mura defect.

where $C(u, v)$ is the coefficient of DCT and $C_{hv}(u, v)$ is the proposed filter.

To verify the effectiveness of the proposed filter in separating the background image from mura defects, an example of reconstructing background images using DCT is illustrated in figure 7. A natural area mura of circular shape is located approximately at the bottom-left corner within the FOS of the LCD. By using the DCT with the proposed filtering strategy, the background image without mura defects was effectively reconstructed. However, it was also observed that the reconstructed image was contaminated by undesired image stripes running horizontally and vertically throughout the mura region detected. This could affect the effectiveness in extracting mura from the background because unexpected stripes could be residual in the inspection results.

Meanwhile, it is important to explain the reason why the reconstructed image can be contaminated by the spurious image stripes when keeping all of the principal frequency along the u and v directions in the DCT. It is interesting to observe that a non-uniform image region such as a mura defect tends to spread its energy according to the image strip orientation of the basic frequency component when it is performed by the DCT. This negative effect becomes significant when the frequency of the principal frequency component is increased more than the spatial frequency of the background image. This undesirable situation should be avoided by further redesigning an effective low-pass filter.

To address the above problem, the proposed filter strategy was modified to select an adequate cut-off frequency along the u and v directions, as shown in figure 8. It is crucial to determine an adequate cut-off frequency along the u and v directions, so that the above-mentioned noise can be avoided. To investigate this, an LCD image containing a natural area

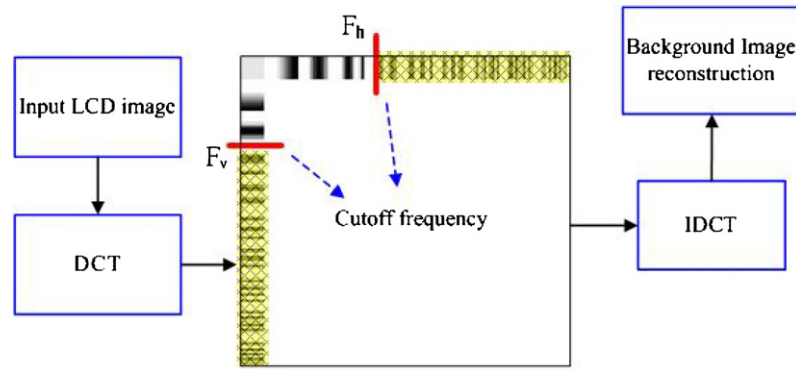


Figure 8. The modified filter designed by a cut-off frequency along the horizontal and vertical axes.

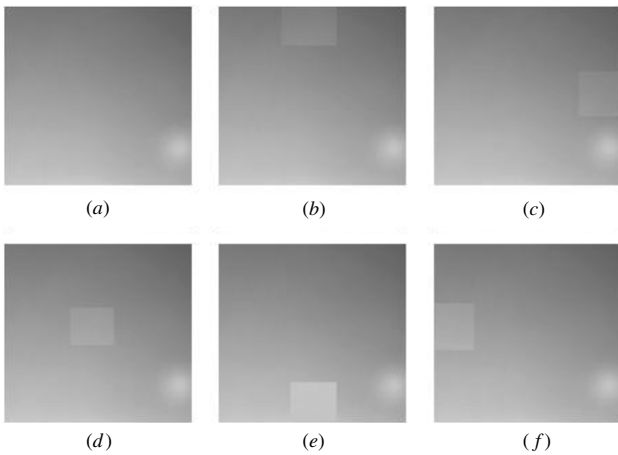
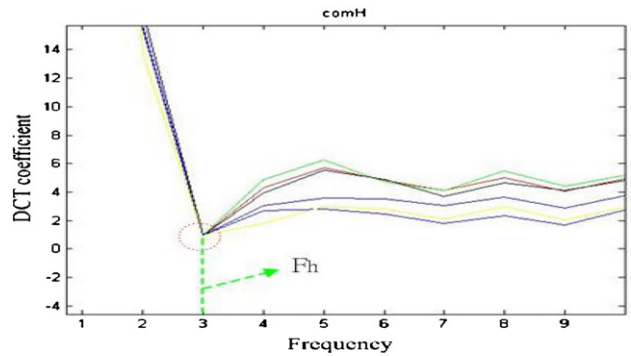


Figure 9. Six FOS images, each having one natural area mura and one artificial defect located at various positions.

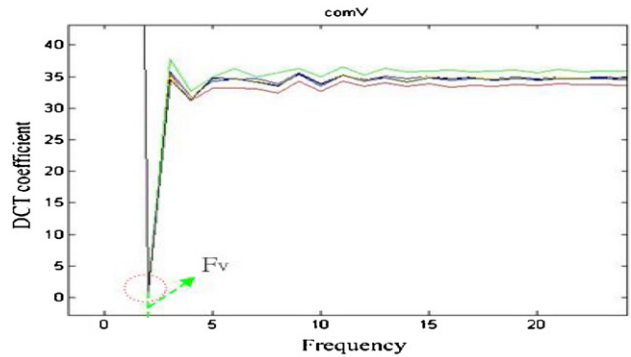
mura was taken as a typical inspection example, where the image was mixed with or without an artificial area mura at five various positions (shown in figure 9). By carefully analyzing their DCT coefficients in the u and v directions, it is amazing to find one and only one distinct transition point at the end of the first continuous slope for all six cases, as shown in figure 10. This distinct point in the u or v direction remains stationary and does not shift or move regardless of the mura positions or defect types, natural or artificial. This reasonably suggests that the spatial frequency content of the background image underlying inspection is mainly retained within these two distinct frequency points (F_h and F_v) along the u and v directions. Therefore, detecting and employing F_h and F_v along the u and v directions as a cut-off frequency for selecting the principal background image component, the background image can be effectively reconstructed without generating the above-mentioned noise. Furthermore, due to the distinct and unique position for each tested image, it is easy to detect these cut-off frequencies. The modified filter is expressed as follows:

$$C_B(u, v) = \begin{cases} C_{hv}(u, v), & u < F_v \text{ or } v < F_h, \\ 0, & \text{otherwise.} \end{cases} \quad (7)$$

The background image ($f_b(x, y)$) can be reconstructed using the following IDCT with the proposed filtering



(a) $C(u,0)$ of DCT in u direction



(b) $C(0,v)$ of DCT in v direction

Figure 10. DCT coefficients both in horizontal and vertical directions for six FOS images with mura defects located at different positions in figures 9(a)–(f).

strategy [10]:

$$f_B(x, y) = \sum_{u=0}^{M-1} \sum_{v=0}^{N-1} \alpha(u)\alpha(v)C_B(u, v) \times \cos\left[\frac{\pi(2x+1)u}{2M}\right] \cos\left[\frac{\pi(2y+1)v}{2N}\right]. \quad (8)$$

Following this, Otsu's global automatic image thresholding method is employed to segment mura defects effectively from the subtracted net image [11]. A between-class-variance-computation (BCVC) architecture is developed to satisfy the high-speed requirements in meeting short tact time. The architecture design of the BCVC employs

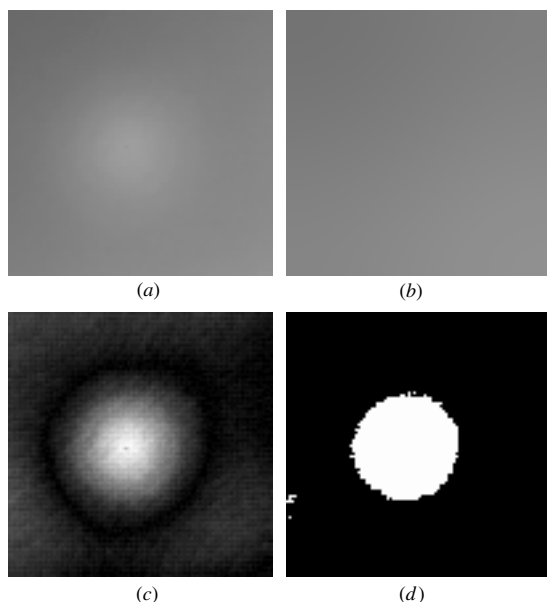


Figure 11. Detection results using the modified filter proposed in figure 10: (a) the original image; (b) the reconstructed background image; (c) the net image; and (d) the detected mura defect.

logarithmic conversion using small LUT and computation units to minimize the bottleneck of finding the maximum between-class variance in Otsu’s method [11]. The proposed implementation is mainly used to eliminate the complex multiplication required in Otsu’s procedure. An LCD image having a natural area mura was taken as an example to test the proposed method. In figure 11, the reconstructed background image is clear from contamination with any stripe noise. The mura defect can be effectively detected by the modified filtering method. The required processing time can be controlled to be within less than 30 ms for a 256 by 256 panel image in a personal computer with an AMD CPU of 2.08 G and 212 MB RAM.

Compared with the original tested image, the background image reconstructed tends to be blurred due to its high-frequency components being removed. The background image only contains the principal background image components which are less than the detected cut-off frequency (F_h and F_v along the u and v directions). The mura defect can be

detected as a regional non-uniform image which has a spatial frequency larger than that of the background image.

3.4. Defect quantification

The difference between the reconstructed background image and the LCD image underlying the inspection can be obtained simply by image subtraction. The result from the subtraction may contain mura defects of various significant levels. It is difficult to determine a quantitative level for panel quality in a complicated multiple-maker and user market. Thus, using the ergonomics approach to investigate the human eye’s sensitivity regarding mura and to express the relation between mura area and image contrast becomes one of the most effective methods for establishing an index to express the level of mura [12]. The detected result obtained using image subtraction is further evaluated by using the Semiconductor Equipment and Materials International (SEMI) formula with the just noticeable difference (JND) definition for mura quantification. The Semu value can be defined as follows [12]:

$$\text{Semu} = \frac{|C_X|}{C_{\text{jnd}}} = \frac{\frac{|I_M - I_B|}{I_B}}{\frac{1.97}{S^{0.33+0.72}}} \quad (9)$$

where C_X is the image contrast; C_{jnd} is the minimum contrast limit for detection; S is the mura area size (pixel); I_M is the image average intensity of the mura region; I_B is the image average intensity of the background region.

Using the ergonomics approach, the above Semu index defines the human eye’s sensitivity regarding mura and quantifies the level of mura by expressing the relation between mura area and contrast. A regressive relationship (C_{jnd} , the minimum contrast limit for detection) is defined between the mura area and the contrast for the human mura JND. The contrast at JND inversely proportional to the mura area raised to the 0.33 power indicates that when the mura area becomes smaller, only darker muras can be sensed [12]. Thus, Semu is defined as a comparison ratio between the contrast of the measurement target and the one in a JND.

From an ergonomic viewing distance, the SEMI standard is normalized so that the unit of Semu represents a just noticeable defect. In the approach, the Semu value can be accurately applied as the threshold to evaluate if any potential mura region being detected is significant to the industrial inspection standard. Figure 12 illustrates an example of

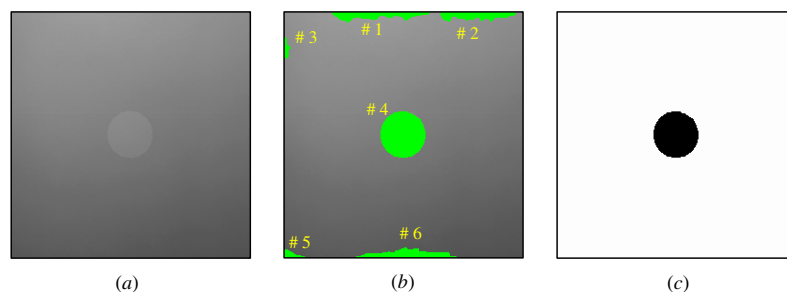


Figure 12. Example of evaluating mura defects using the SEMI standard: (a) the original image; (b) the suspected defect regions being identified by the proposed method; and (c) the mura defect detected after being quantified by the SEMI standard.

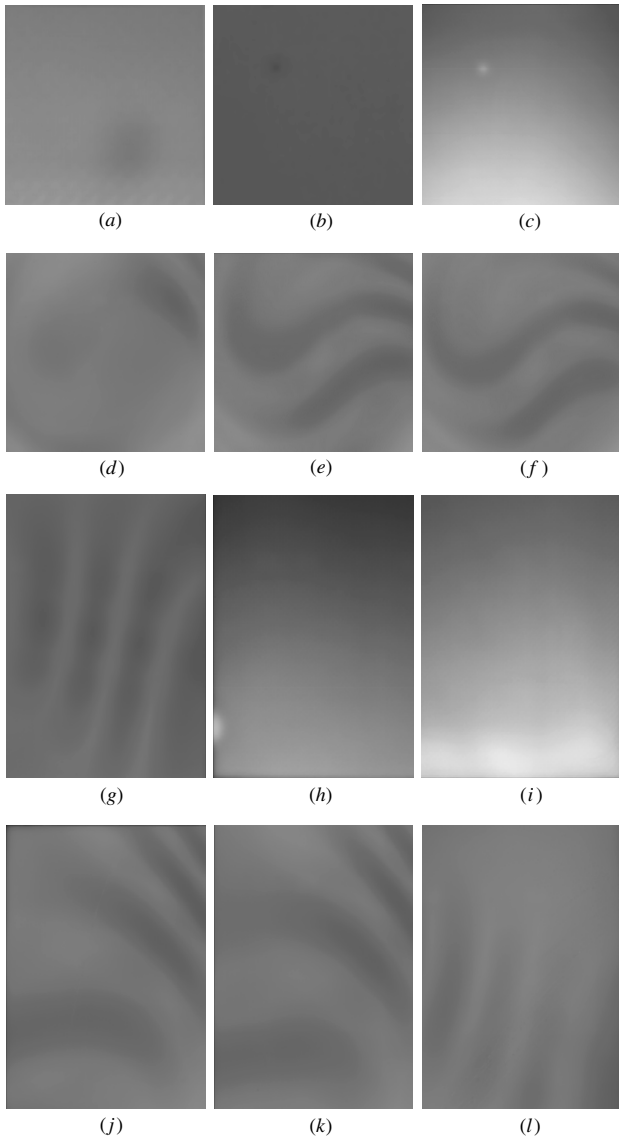


Figure 13. LCD panel images with natural mura defects: (a)–(l) are the original images to be inspected.

Table 1. Semu evaluation results of the LCD inspection example shown in figure 13.

Defect index	S (pixels)	C_x (%)	C_{ind} (%)	Semu
1	221	0.42	1.05	0.40
2	232	0.29	1.04	0.27
3	18	0.59	1.47	0.40
4	1824	8.04	0.88	9.09
5	259	0.38	1.03	0.37
6	19	0.83	1.46	0.57

LCD image inspection, where six susceptible (or potential) image regions were first detected by the approach and further evaluated automatically by the SEMI standard. Table 1 shows that only defect 4 was significant (shown in figure 12(c)) and the remaining susceptible regions (defects 1–3) were

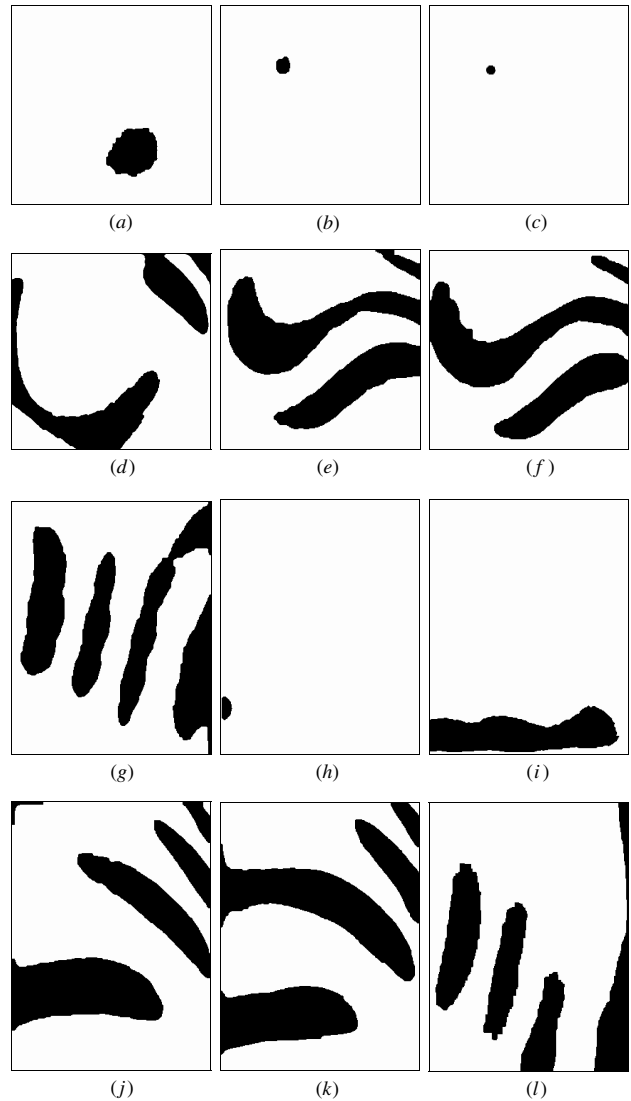


Figure 14. Inspection results of LCD panel images with natural mura defects: (a)–(l) are the detected mura defects.

eliminated when the threshold of the quantification was set at 1.

4. Experimental results and discussion

The actual performance of the developed method was evaluated on industrial LCD panels containing natural mura defects provided by a local TFT/LCD manufacturer. The developed method was employed to detect six cases of natural low-contrast mura, as shown in figure 13. Figures 13(a)–(l) are the original LCD images containing natural mura defects. When using the background reconstruction method, the background images were first reconstructed by the DCT method effectively. With the developed detection method, the mura defects originally contained in these LCD images were successfully detected and shown in figures 14(a)–(l). These experimental results indicate that the developed methodology

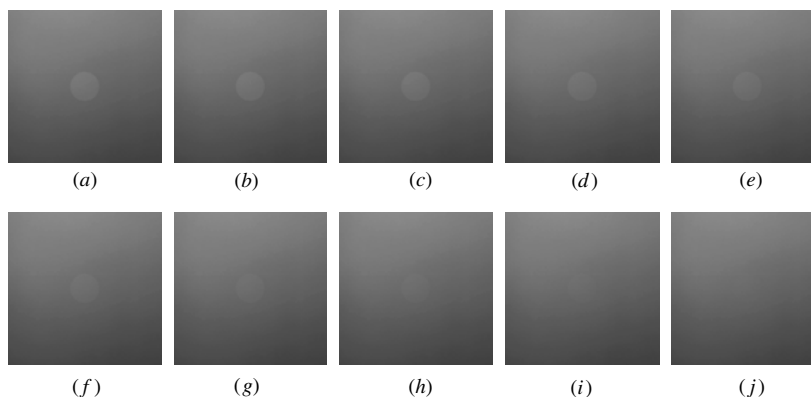


Figure 15. Ten different gray-value levels of artificial circular mura defects being added into an LCD panel having a common gray distribution, in which the differences in gray value range from 10 to 1, respectively.

Table 2. Semu evaluation results of the LCD inspection example shown in figure 15.

Gray-value difference	$ C_x $ (%)	C_{jnd} (%)	Semu value	Inspection quality
10	8.32	0.88	9.3	●
9	7.42	0.88	8.39	●
8	6.61	0.88	7.48	●
7	5.79	0.88	6.55	●
6	4.78	0.88	5.39	●
5	3.07	0.89	3.44	●
4	0.52	1.22	0.43	□
3	0.48	1.28	0.31	□
2	0.37	1.28	0.29	□
1	0.18	1.5	0.12	□

Inspection quality: ● Good □ Fail.

is capable of automatic mura defect detection. From the proposed method, a BCB C++ program was developed in a personal computer with an AMD CPU of 2.08 G and 212 MB RAM. An LCD image frame inspection with a size of 256×256 pixels² can be accomplished in less than 75 ms. Mura defect detection can be accomplished in a short time frame, thus satisfying requirements for short tact time for the on-line field application of FOS quality inspection.

Meanwhile, it is also important to investigate the minimum detectable gray-level difference between mura defects and background images using the developed methodology. To achieve this, ten different gray-value levels of artificial circular mura defects were added to an LCD panel having common gray distribution, in which the differences in gray values ranged from 10 down to 1, as shown in figure 15. The Semu evaluation results obtained by the

proposed inspection approach are displayed in table 2. It was clearly identified that the minimum detectable gray-level difference between mura defects and background was five. Experimental results reveal that decreasing the cut-off frequency (F_h and F_v) should enhance the sensitivity of defect detection, especially when the gray-value difference is small. However, by doing so, undesired image stripes which ran horizontally and vertically throughout the mura region could again appear in the reconstructed background image. This could also increase the difficulties in the image processing required by defect segmentation and quantification.

Comparison was made between the proposed method and the other two mura detection methods reported in the literature review [4, 5]. As seen in table 3, the DCT and Lee and Yoo’s method have a similar sensitivity in the minimum detectable contrast while Kim and Yoon’s method is slightly better but limited to non-stripe defects. Moreover, the DCT method is superior in detection efficiency while its detectable defect morphology can be arbitrary.

5. Conclusions

A novel background image reconstruction methodology was developed according to the DCT principle and image filtering strategy to establish the background portion of the LCD image separated from mura defects. The developed method applies the intrinsic properties of the frequency characteristics of area muras to extract low-contrast muras from non-uniform background images. The experimental results performed on natural mura defects indicate that the established TFT-LCD defect detection methodology is capable

Table 3. Comparison of three kinds of inspection methods.

	Defect morphology	Minimum detectable contrast difference	Inspection time required (ms)	Detecting principle
Kim and Yoon [5]	Any kind of shape except stripes	4	150	Brightness flattening
Lee and Yoo [4]	Any kind of shape	8	60 000	Background data fitting
DCT method	Any kind of shape	5	75	Discrete cosine transform

Hardware condition: a personal computer with an AMD CPU of 2.08 GHz and 212 MB RAM.

of performing automatic detection of mura defects with low-contrast brightness down to a five gray-value level. Meanwhile, the method can be operated efficiently completing the inspection of a 256 by 256 image in less than 75 ms. The method has also been proved to be effective in detecting various categories of mura with different region sizes, shapes and contrasts. Moreover, the detected defect regions can be accurately quantified to determine the noticeable significance of human visual performance.

Acknowledgment

The authors would like to thank the National Science Council of Taiwan, for financially supporting this research under grant NSC 94-2212-E-027-016.

References

- [1] Kuo C-C 2006 TFT-LCD mura defect detection using DCT and filtering strategy *Master Thesis* National Taipei University of Technology
- [2] Chen L-C, Yang S-L, Kao C-C and Huang Y-T 2005 *J. Chin. Soc. Mech. Eng.* **26** 785–9
- [3] Song Y C, Choi D H and Park K H 2004 *Japan. J. Appl. Phys.* **43** 5465–8
- [4] Lee J Y and Yoo S I 2004 *IEICE T. Inf. Syst.* **E87-D** 2371–8
- [5] Kim S W and Yoon D S 1999 Rapid defect of display devices with optical spatial filtering *Proc. SPIE* **3824** 255–61 (Germany)
- [6] Yen T-C and Tso P-L 2004 *J. Micromech. Microeng.* **14** 867–75
- [7] Ahmed N, Natarajan T and Rao K R 1974 *IEEE Trans. Comput.* **23** 90–3
- [8] Pennebaker W B and Mitchell J L 1993 *JPEG—Still Image Data Compression Standard* (New York: International Thomson Publishing)
- [9] Khayam S A 2003 *The Discrete Cosine Transform (DCT): Theory and Application (Seminar Note)* (Michigan State University)
- [10] Chen L-C and Kuo C-C 2006 23–5 TFT-LCD mura defect detection based on discrete cosine transform and filtering strategy *The International Manufacturing Leaders Forum (Taiwan)*
- [11] Tian H, Lam S K and Srikanthan T 2003 Implementing Otsu's thresholding process using area-time efficient logarithmic approximation unit *Proc. 2003 Int. Symp. on Circuits and Systems vol 4 (Japan)* IV-21–4
- [12] SEMI 2006 *Definition of measurement index (SEMU) for luminance mura in FPD image quality inspection* (SEMI D31–1102, Semiconductor Equipment and Materials International)